MOTION-INDUCED VORTEX VIBRATION OF A DIAGONAL MEMBER IN A STEEL TRUSS BRIDGE

K. Matsuda*, K. Kato*, N. Cao*, K. Shigetomi* and K. Ejiri*

* Kyushu Institute of Technology, Japan
e-mails: matsuda@civil.kyutech.ac.jp, kato.kusuo78o@mail.kyutech.jp,
cao.nade133@mail.kyutech.jp, p105037k@mail.kyutech.jp, ejiri.kazufumi221@mail.kyutech.jp

Abstract. *In 2009, Ikitsuki Bridge, a truss bridge in Nagasaki Prefecture with a center span length of 400 m, was discovered to have a crack in the diagonal member of the bridge. The side ratio of the section was B/D=1.18. Since motion-induced vortex vibration has not been confirmed on rectangular cross sections with side ratios of B/D<2 according to the past wind tunnel tests, wind tunnel tests were carried out. The tests had an additional purpose of clarifying the effects of the small protruding lips of flanges in steel structures on motion-induced vortex vibration. Spring-supported tests, smoke flow visualizations were performed with or without small protruding lips of flanges changing angle of attack. It was found that motion-induced vortex vibration were confirmed with a rectangular cross section with a side ratio of B/D=1.18 by experimental results of a spring-supported tests, an unsteady aerodynamic lift measurement and a flow visualization test. The effects of the existence of small protruding lips of flanges became large when angle of attack became greater than 3-4 degrees.*

1 INTRODUCTION

The vortices separated from rectangular cross sections are broadly classified into Kármán vortices and motion-induced vortices (vortices separated from the leading edge) [1, 2]. The former are those that are accompanied by the interferences of two separated shear layers at both the top and bottom surfaces of the structures. The latter are the ones that are shedding separately from the leading edges of the top and bottom surfaces caused by the separated shear layers at the top and bottom surfaces excited alternately due to the vibration of the rectangular cross section. The vibration caused by the latter vortices was found in past wind tunnel tests [3, 4]. The vibration is known as either motion-induced vortex vibration [1, 2] or impinging-shear-layer instability [5-8]. The onset wind speed of this vibration depends on the side ratio of the rectangular cross section and this relationship is schematically clarified [1, 8]. The mechanisms of the motion-induced vortex vibration of the rectangular section and H-shaped section cylinders are also revealed [9-12]. This research is involved in the motion-induced vortex vibration generated in a bracing member of a real truss bridge in Japan.

In 2009, Ikitsuki Bridge, a truss bridge in Nagasaki Prefecture with a center span length of 400 m, was discovered to have a crack in the diagonal member of the bridge [13]. The side ratio of the section was *B/D*=1.18 (*B*: along-wind length, 590mm, *D*: cross-wind length, 500mm). As a result of a field oscillation measurement, the primary cause of the crack was identified as Kármán vortex vibration. However, another aerodynamic vibration was also observed in the wind speed range lower than the resonance wind speed of the Kármán vortex vibration. Since the Scruton number of the bracing members was estimated to be approximately 2-3, the aerodynamic vibration was initially thought to be motion-induced vortex vibration. The Scruton number is defined as $Sc=2m\delta/(\rho D^2)$, in which m= mass of the structure per length; δ=structural damping (logarithmic decrement) measured in still air; ρ=air density. The generation of motion-induced vortex vibration is considered to be caused by the unification of separated vortices from the leading edge and secondary vortices at the trailing edge [1]. Though motion-induced vortex vibration has been confirmed on rectangular cross sections with side ratios of *B/D*=2–8 according to the results of past wind tunnel tests, there is little past research on motion-induced vortex vibration on a rectangular cross section of *B/D* of less than 2. For that reason, wind tunnel tests for *B/D*=1.18 was conducted to simulate the phenomenon in a closed circuit wind tunnel at Kyushu Institute of Technology. A new finding was that the vibration in the bracing member with a rectangular cross section (*B/D*=1.18) of Ikitsuki Bridge generated in the wind speed range of lower than Kármán vortex-induced vibration was suggested to possibly be motion-induced vortex vibration by the experimental results of the spring-supported test, the unsteady aerodynamic lift measurement and the flow visualization [14-17].
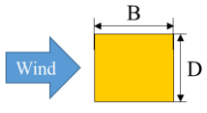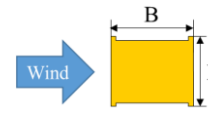
In this paper, the authors focused on the wind tunnel model configuration. Small protruding lips of flanges in steel structures have not been usually taken into consideration when manufacturing wind tunnel test models. Wind tunnel tests were carried out in order to clarify the effects of the existence of small protruding lips of flanges in steel structures on motion-induced vortex vibration. Spring-supported tests, smoke flow visualizations and Strouhal number measurement were performed with or without small protruding lips of flanges changing angle of attack. Models were forced-oscillating in smoke flow visualizations and unsteady aerodynamic lift measurements. All wind tunnel tests were conducted in a smooth flow.

2 EXPERIMENTAL SETUP

2.1 Section Models

Table 1 shows the dimensional data of the section models, *B/D*=1.18, used in each test. Two cross-sections of a rectangular cross-section and a cross-section with flanges, a reproduction of the cross-section of the cracked bracing member of Ikitsuki Bridge, were used. "Flanges" here means the small protruding lips of the flanges.

Table 1. Section models (*B/D*=1.18)

Wind Tunnel Tests	Without Flanges		With Flanges	
	B(mm)	*D*(mm)	*B*(mm)	D(mm)
Spring-Supported Tests	107	90.0	107	90.0
Flow Visualization Tests	47.2	40.0	47.2	40.0

2.2 Spring-supported Tests

The spring-supported test was conducted in a closed circuit wind tunnel (cross-section:1.8m high×0.9m wide) at Kyushu Institute of Technology. Table 2 shows the conditions for the spring-supported test. The primary experimental conditions for the model were: mass per unit length=3.32, 3.01 kg/m, natural frequency of heaving vibration=7.30, 7.69 Hz, logarithmic decrement of structural damping=0.0033, 0.0036 and Scruton number=2.23-2.29. Figure 1 shows a photo of the section model installed in the wind tunnel.

Table 2. Spring-supported test conditions

	Without Flanges	With Flanges
Angle of attack, α	3,4,5 deg.	
Mass per unit length, m	3.32 kg/m	3.01 kg/m
Natural frequency, f	7.30 Hz	7.69Hz
Structural damping (in logarithmic decrement), δ	0.0033	0.0036
air density: ρ	1.18-1.20 kg/m^3	1.19-1.20 kg/m^3
Scruton number, $Sc=2m\delta/\rho D^2$	2.25-2.29	2.23-2.25

D: Model height =0.090m, *L*: Model length=0.768m

Figure 1. Section model for spring-supported tests mounted in Kyushu Institute Technology wind tunnel

2.3 Flow Visualization Tests

Figure 2 shows the experimental system of the flow visualization tests. Flow visualizations around the model during static and oscillating times were conducted using a small-sized wind tunnel (0.4m high×0.4m wide) at Kyushu Institute of Technology. It was considered that the wind speeds in the wind tunnel of *V*=0.6-1.0 m/s are good for visualization, so *V*=0.6 m/s was selected. Accordingly, the experimental Reynolds number was *Re*=*VD/v*=1.6×10^3. The forced-oscillating non-dimensional amplitudes *2η/D* were selected in accordance with the spring-supported test results. Figures 3 and 4 show the forced oscillation system and the installation status of the model, respectively. Table 3 shows the conditions for the flow field visualization tests.
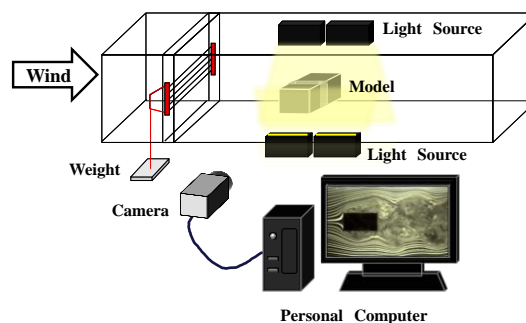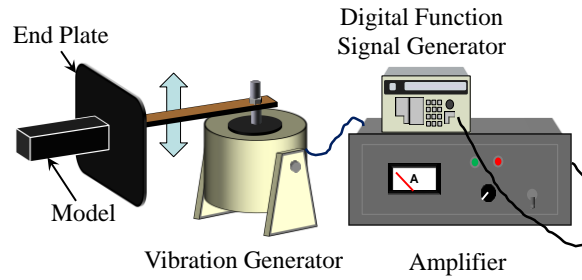

Figure 2. Flow visualization test system

Figure 3. Forced oscillation system for flow visualization tests
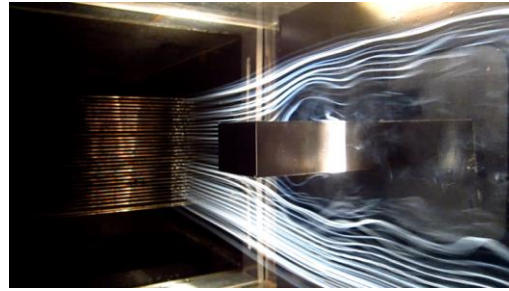

Figure 4. Section model for flow field visualization test mounted in Kyushu Institute Technology wind tunnel

Table 3. Flow visualization test conditions

	Wind speed region around Motion-induced vortex vibration	Wind speed region of Kármán vortex-induced vibration	Wind speed region of Galloping
Angle of attack, α	0,3,4,5,10 deg.	0,5,10 deg.	
Wind speed, V	0.6 m/s		
Frequency of forced oscillation method, f	5.0 Hz	1.95, 1.79 Hz	1.07 Hz
Reduced wind speed, $Vr=V/fD$	3.0	7.70, 8.40	14.0
Forced-oscillating non-dimensional amplitudes, $2\eta/D$	0.10	0.10	0.15

D: Model height =0.040m, L: Model length=0.150m

3   EXPERIMENTAL RESULTS AND DISCUSSION

3.1 Spring-supported Tests

Figure 5 shows the result of the spring-supported test for an angle of attack of 0 degrees [14,15]. Vibrations were confirmed from the neighborhoods of reduced wind speed Vr=2 and 8. Because the reduced wind speed at motion-induced vortex vibration is calculated as Vr=1.67×B/D=1.67×1.18=2.0 [1], vibrations around Vr=2 were considered to be motion-induced vortex vibration. The effects of the existence or non-existence of flanges on the maximum response amplitude of motion-induced vortex vibration are extremely small. However, Figure 6 shows the result of an experiment separately conducted with an angle of attack of 10 degrees that the maximum response amplitude of motion-induced vortex vibration in the case with flanges was approximately 1.5 times larger than that in the case with no flange. Moreover, the responses over the reduced wind speed of Vr=10 were quite different. The response of the model with flanges was much larger than without flanges. In other words, it turns out that as the angle of attack becomes larger, the existence or non-existence of flanges tends to exercise an effect on the patterns of the flows around the cross-section.

The Strouhal number measured on the cross-section with flanges was St=0.124. Its inverse number is the critical reduced wind speed of beginning Kármán vortex-induced vibration, Vr=1/St=8.1. In other words, a vibration beginning in the neighborhood of a reduced wind speed of 8 can be judged as Kármán vortex-induced vibration. However, from the fact that the Scruton number in this experiment's case was small at Sc=1.32, it was found that Kármán vortex-induced vibration was changed to a galloping along with the increase in wind speed.

Based on the above experimental results [14,15], additional wind tunnel tests were carried out in order to clarify the effects of rectangular column flanges in this study.
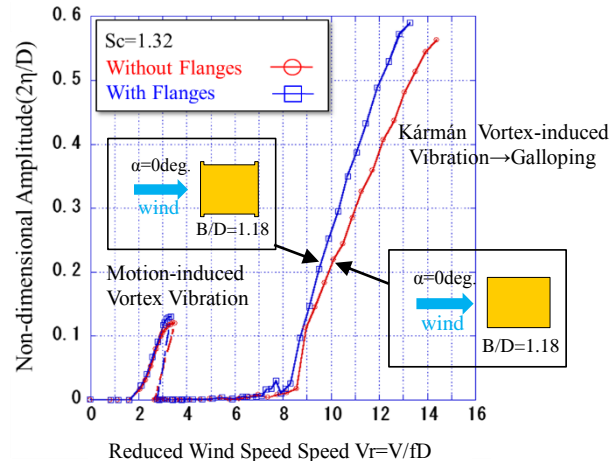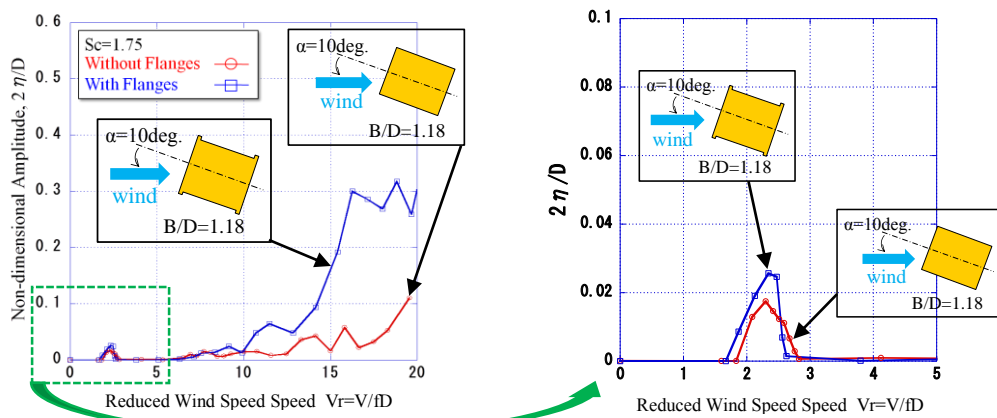
Figure 5. Spring-supported test result (α=0 deg.)[14, 15]

Figure 6. Spring-supported test result (α=10 deg.)[14, 15]

Figures 7, 8 and 9 show the results of the spring-supported test for angles of attack of 3, 4 and 5 degrees, respectively. The ratios of the response amplitude of motion-induced vortex vibration with flanges compared to without flanges at angles of attack of 3, 4 and 5 degrees were approximately 1.0, 1.2 and 1.6, respectively. The effects of the existence of flanges became large when angle of attack became greater than 3-4 degrees.

In other words, as the angle of attack becomes larger, the existence or non-existence of flanges tends to have an effect on the patterns of flows around the cross section. On the other hand, the effect of the flange on Kármán vortex-induced vibration and galloping was hardly seen. As will be described later, discussion will be given to these causes based on the flow visualization test results.

It was found that it could be very important to model small protruding lips of flanges in steel structures for wind tunnel tests, especially bracing members of long-spanned truss bridges from a wind engineering point of view.
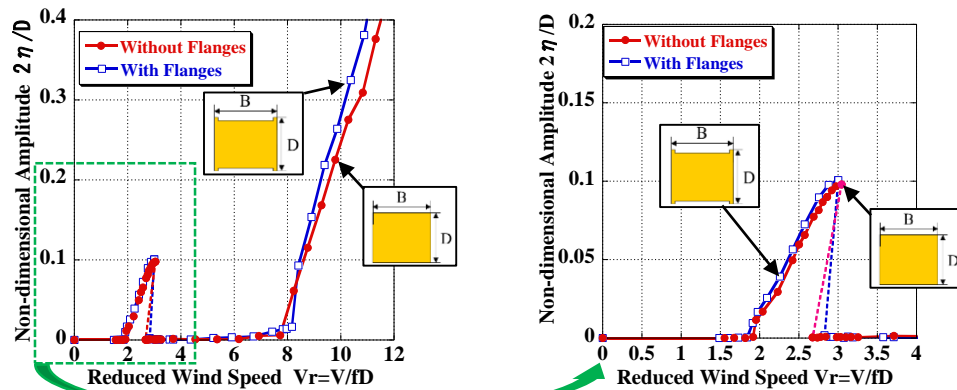
Figure 7. Spring-supported test result (α=3 deg.)
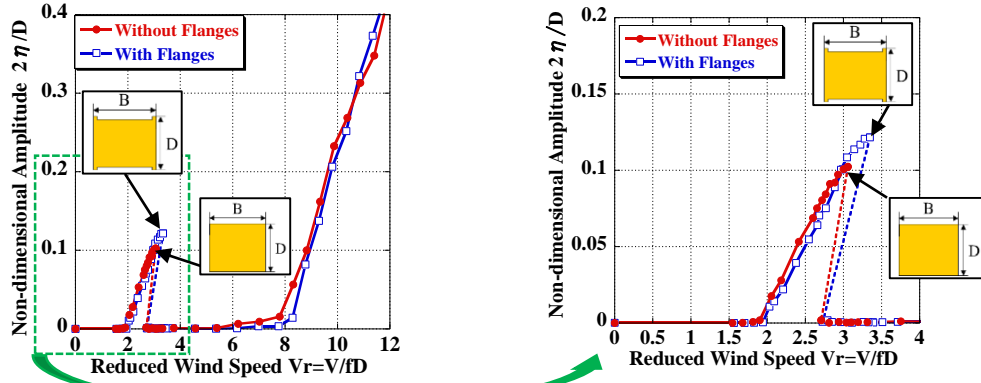
Figure 8. Spring-supported test result (α=4 deg.)
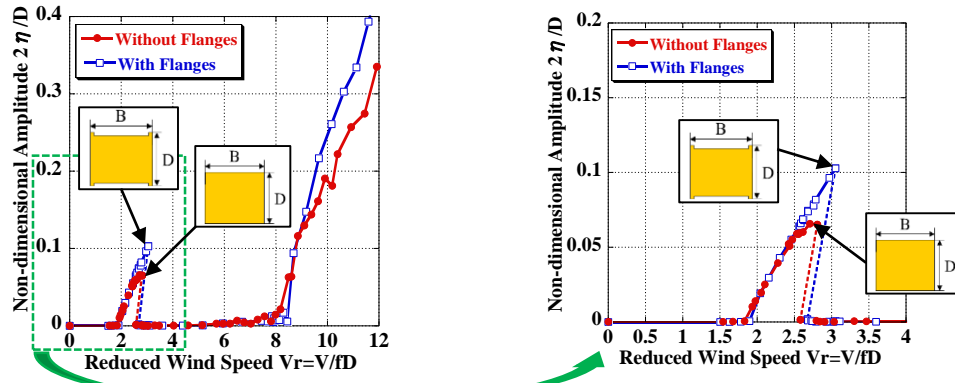
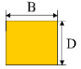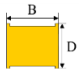Figure 9. Spring-supported test result (α=5 deg.)

3.2 Flow Visualization Tests

Figure 10 shows the results of flow visualization tests around forced-oscillating rectangular section models of B/D=1.18 at the top displacement at the maximum response wind speed of motion-induced vortex vibration. It was confirmed that as the angle of attack becomes larger, the formation of separated vortex from the leading edge on the lower surface of the model with flanges is larger than that without flanges. Generally, it is clear that the pressure tends to decrease in the vicinity of the center of the vortex as compared with the surroundings. Therefore, the larger the separated vortex from the leading edge becomes, the larger the negative pressure on the lower surface becomes. It is supposed that the exciting force acting on the lower surface becomes larger. The separated vortex from the leading edge gradually separated from the upper surface of the cross sections and flowed downward as the angle of attack became larger.

Results of flow visualization tests around forced-oscillating rectangular section models of B/D=1.18 at the top displacement in the wind speed region of Kármán vortex-induced vibration is shown in the upper half of Figure 11. Even if the angle of attack becomes larger, the effects of the existence or non-existence of flanges on the flow pattern around the section model were hardly seen. Table 4 shows measured Strouhal number changing angle of attack. The effects were also not seen in the predominant vortex shedding frequency.

Results of the flow visualization tests around the forced-oscillating rectangular section models of B/D=1.18 at the top displacement in the wind speed region of galloping is shown in the lower half of Figure 11. Though the difference of flow patterns under the lower surface of the model between with and without flanges was not recognized at an angle of attack of 0 degrees, a larger flow separation occurs from the leading edge of the lower surface with flanges than that without flanges at an angle of attack of 10 degrees. Quantitatively showing this fact is unsteady aerodynamic lift $C_{L\eta i}$ in Figures 12 and 13 to be described later. Unsteady aerodynamic lift coefficients $C_{L\eta i}$ with flanges around Vr=14.0 at an angle of attack of 10 degrees as shown in Figure 13 are positive values which means the exciting force is acting on the surface, while $C_{L\eta i}$ without flanges are negative values. Therefore, the response with flanges becomes larger than that without flanges.

Table 4. Measured Strouhal Number $St=fD/V$

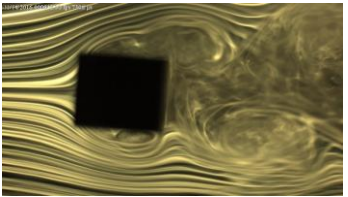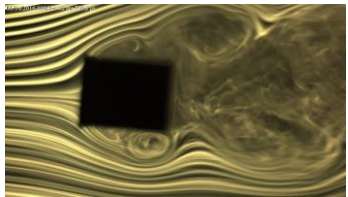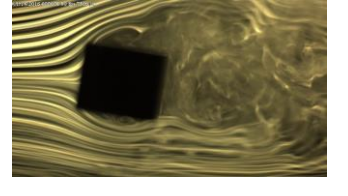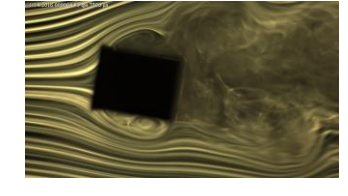| Cross Sections	Angle of Attack $α$ (deg.)				
	0	3	4	5	10
![B D]	0.120	0.120	0.120	0.120	0.132
![B D]	0.121	0.121	0.122	0.122	0.131
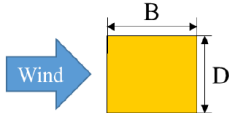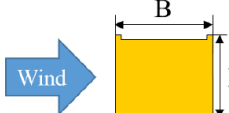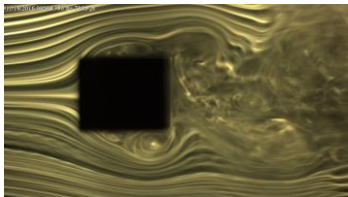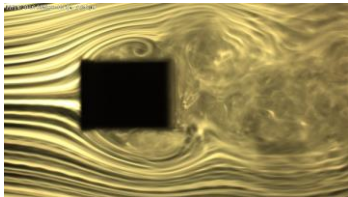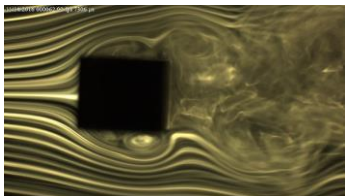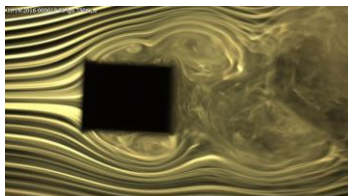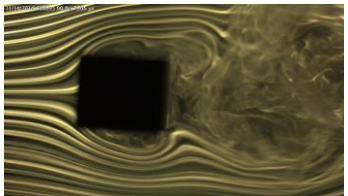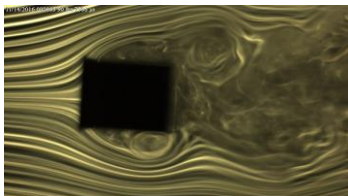
Reduced Wind Speed $Vr=V/fD$	Non-dimensional Forced-Oscillating Amplitude $2\eta/D$	Angle of Attack (deg.)	Without Flanges	With Flanges
3.0	0.10	0		
		3		
		4		
		5		
		10		

Figure 10. Results of flow visualization tests around forced-oscillating rectangular section models of *B/D*=1.18 at the top displacement at the maximum response wind speed of motion-induced vortex vibration
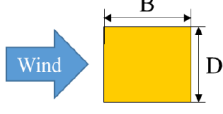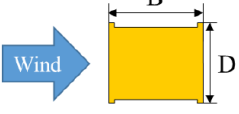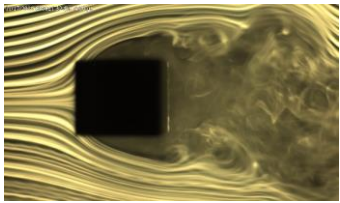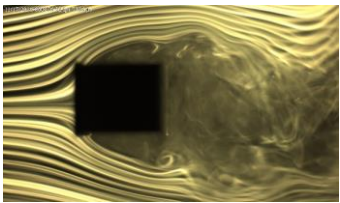
Reduced Wind Speed $Vr=V/fD$	Non-dimensional Forced-Oscillating Amplitude $2\eta/D$	Angle of Attack α (deg.)	Without Flanges	With Flanges
$Vr=8.40$ ($\alpha=0,5$ deg.) $Vr=7.70$ ($\alpha=10$ deg.) Wind speed region of Kármán vortex-induced vibration	0.10	0		
		5		
		10		
$Vr=14.0$ Wind speed region of Galloping	0.15	0		
		5		
		10		

Figure 11. Results of flow visualization tests around forced-oscillating rectangular section models of *B/D*=1.18 at the top displacement in the wind speed regions of Kármán vortex-induced vibration and galloping

3.3 Unsteady Aerodynamic Lift Measurements

The unsteady aerodynamic lift obtained by the forced oscillation method is shown by the following equation:

$$Lift = \pi \rho D^3 \omega^2 \left(C_{L\eta R} + iC_{L\eta i}\right)\frac{\eta}{D} \tag{1}$$

where *Lift* is the unsteady aerodynamic lift per unit length [N/m], ρ: air density [kg/m^3], ω: circular frequency of the forced oscillation [rad/s], $C_{L\eta R}$: real part of unsteady aerodynamic lift coefficients, $C_{L\eta i}$: imaginary part of unsteady aerodynamic lift coefficients, η=vertical oscillation amplitude [m] and D: height of model [m].

Substituting equation (1) into the external force term of the Equation of Motion and obtaining the following equations:

$$m\ddot{\eta} + c\dot{\eta} + k\eta = \pi \rho D^3 \omega^2 \left\{\left(C_{L\eta R} + iC_{L\eta i}\right)\frac{\eta}{D}\right\} \tag{2}$$

where *m*=mass, *c*=damping coefficient, *k*= stiffness.

$$m\ddot{\eta} + (c - \pi \rho D^2 \omega C_{L\eta i})\dot{\eta} + (k - \pi \rho D^2 \omega^2 C_{L\eta R})\eta = 0 \tag{3}$$

$$c - \pi \rho D^2 \omega C_{L\eta i} < 0 \tag{4}$$

Accordingly, from equation (4), if the damping constant, *c* is very small, and $C_{L\eta I}$ is a positive value, it means that the structure is aerodynamically unstable.

Figure 12 shows unsteady aerodynamic lift coefficients $C_{L\eta i}$ at an angle of attack of 0 degrees and an enlarged view in the wind speed range of *Vr*=0-5[14,15]. $C_{L\eta i}$ in the ranges of the wind speed of motion-induced vortex vibration and Kármán vortex-induced vibration are positive values and they correspond to the responses in Figure 5. This shows the same tendency as the result that was confirmed by Yagi et al. [18], indicating that unsteady aerodynamic force coefficient $H_1{}^*$ of rectangular cross-section *B/D*=1 becomes a positive value in the neighborhoods of *Vr*=1.67×*B/D*=1.67 and *Vr*=1/*St*. Furthermore, Nakamura and Mizota suggested the existence of low speed instability from the results of measuring unsteady aerodynamic lifts using a rectangular cross section of *B/D*=1 [19, 20].

According to Figure 12, there is very small difference between $C_{L\eta i}$ "without flanges" and "with flanges" in the wind speed range of motion-induced vortex vibration at an angle of attack of 0 degrees. Therefore, the effects of the existence or non-existence of flanges on the maximum response amplitude of motion-induced vortex vibration are extremely small.

Figure 13 shows unsteady aerodynamic lift coefficients $C_{L\eta i}$ at an angle of attack of 10 degrees and an enlarged view in the wind speed range of *Vr*=0-5[14,15]. There are some differences between $C_{L\eta i}$ "without flanges" and "with flanges" in the wind speed range of motion-induced vortex vibration and Kármán vortex-induced vibration at an angle of attack of 10 degrees. Unlike the response when an angle of attack is 0 degrees, the responses "with flanges" and "without flanges" greatly differ at an angle of attack of 10 degrees, as shown in Figure 6.
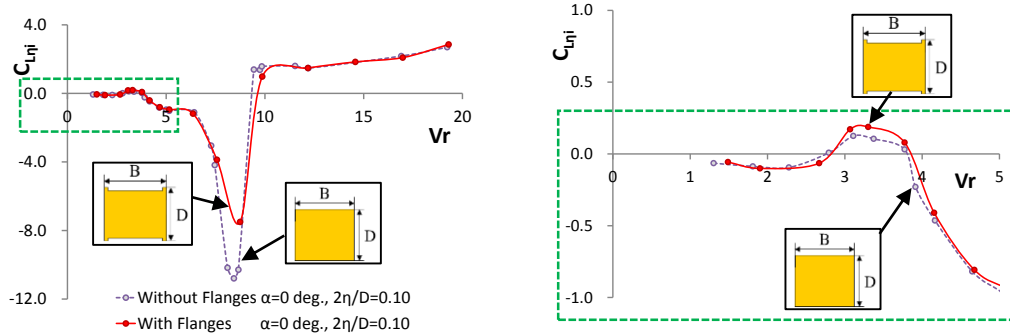

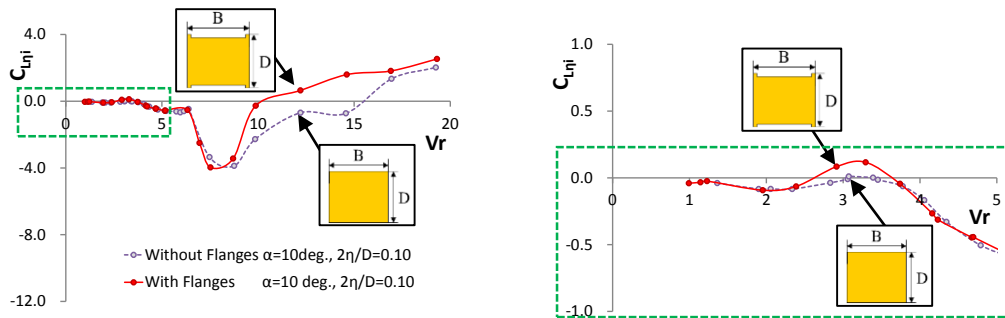Figure 12. Unsteady aerodynamic lift coefficients $C_{L\eta I}$ (α=0deg.) [14,15]

Figure 13. Unsteady aerodynamic lift coefficients $C_{L\eta I}$ (α=10deg.) [14,15]

4 CONCLUSIONS

The findings obtained from this research are as follows:

(1) Though motion-induced vortex vibration has been confirmed on rectangular cross sections with side ratios of *B/D*=2–8 according to the results of past wind tunnel tests, it was found that the motion-induced vortex vibration were confirmed with a rectangular cross section even with a side ratio of *B/D*=1.18 by experimental results of a spring-supported test, an unsteady aerodynamic lift measurement and a flow visualization test.

(2) The effects of the existence of small protruding lips of flanges became large when angle of attack became greater than 3-4 degrees.

(3) According to smoke flow visualization test results, flow patterns around a model with small protruding lips of flanges were different from those around a model without small protruding lips of flanges. Unsteady aerodynamic lifts acting on the models were also different from each other based on the wind tunnel test results.

(4) It could be very important to model small protruding lips of flanges of rectangular columns in steel structures for wind tunnel tests, especially diagonal members of long-spanned truss bridges from a wind engineering point of view.

REFERENCES

[1] N. Shiraishi, M. Matsumoto: On classification of vortex-induced oscillation and its application for bridge structures, *Journal of Wind Engineering and Industrial Aerodynamics*, Vol.14, Nos.1-3, pp.419-430, 1983.

[2] S. Komatsu and H. Kobayashi: Vortex-induced oscillation of bluff cylinders, *Journal of Wind Engineering and Industrial Aerodynamics*, Vol.6, pp.335-362, 1980.

[3] M. Novak: Galloping and vortex induced oscillations of structures, *Proceedings of the Third International Conference on Wind Effects on Buildings and Structures*, Tokyo, Japan, pp.799-809, 1971.

[4] Y. Otsuki, K. Washizu, H. Tomizawa, A. Ohya and K. Fujii: Experiments on the aeroelastic instability of prismatic bars with rectangular sections, *Proceedings of the Third International Conference on Wind Effects on Buildings and Structures*, Tokyo, Japan, pp.891-898, 1971.

[5] D. Rockwell and E. Naudascher: Review- Self-sustaining oscillations of flow past cavities, *Transactions of the ASME, Journal of Fluids Engineering*, Vol.100, pp.152-165, 1978.

[6] Y. Nakamura, Y. Ohya and H. Tsuruta: Experiments on vortex shedding from flat plates with square leading and trailing edge, *Journal of Fluid Mechanics*, Vol. 222, pp.437-447, 1991.

[7] Y. Ohya, Y. Nakamura, S. Ozono, H. Tsuruta and R. Nakayama: A numerical study of vortex shedding from flat plates with square leading and trailing edges, *Journal of Fluid Mechanics*, Vol. 236, pp.445-460, 1992.

[8] E. Naudascher and Y. Wang: Flow-induced vibrations of prismatic bodies and grids of prisms, *Journal of Fluids and Structures*, Vol.7, pp.341-373, 1993.

[9] M. Matsumoto, N. Shiraishi, H. Shirato, S. Stoyanoff, and T. Yagi: Mechanism of, and turbulence effect on vortex-induced oscillations for bridge box girders, *Journal of Wind Engineering and Industrial Aerodynamics*, Vol. 49, Issues 1-3, pp.467-476, 1993.

[10] Y. Kubo, K. Hirata and K. Mikawa: Mechanism of aerodynamic vibrations of shallow bridge girder sections, *Journal of Wind Engineering and Industrial Aerodynamics*, Vol.41-44, pp.1297-1308, 1992.

[11] R. Mills, J. Sheridan, K. Hourigan and M.C. Welsh: The mechanism controlling vortex shedding from rectangular bluff bodies, *Proceedings of the twelfth Australasian Fluid Mechanics Conference*, Sydney, pp.227-230, 1995.

[12] R. Mills, J. Sheridan and K. Hourigan: Particle image velocimetry and visualization of natural and forced flow around rectangular cylinders, *Journal of Fluid Mechanics*, Vol. 478, pp.299-323, 2003.

[13] S. Nakamura, T. Okumatsu, T. Nishikawa and T. Okabayashi : A Fatigue Damage of a Diagonal Member in a Steel Truss Bridge Due to Wind-Induced Vibration, Developments in International Bridge Engineering -Selected Papers from Istanbul Bridge Conference, pp.211-220, 2014.

[14] K. Matsuda, K. Kato, K. Hisadomi and K. Harada: Low speed instability of two-dimensional rectangular prisms, *Proceedings of the ASME 2013 Pressure Vessels and Piping Conference (PVP2013)*, 97353, 2013.

[15] K. Matsuda, K. Kato, Y. Tamai, K. Misawa and I. Ikeda : Experimental Study on Aerodynamic Vibrations of a Bracing Member with a Rectangular Cross Section of The Long–Spanned Truss Bridge, *Proceedings of 14th International Conference on Wind Engineering*, June, 2015.

[16] K. Matsuda, K. Kato, Y. Tamai and K. Suda : Experimental study on aerodynamic vibration of rectangular cross sections having low side ratios, *Proceedings of 8th International Colloquium on Bluff Body Aerodynamics and Applications*, 2016.

[17] K. Matsuda, K. Kato, K. Arise and H. Ishii : Study on the Relation between Side Ratios of Rectangular Cross Sections and Secondary Vortices at Trailing Edge in Motion-induced Vortex Vibration, *Proceedings of the ASME 2017 Pressure Vessels*

& Piping Division Conference (PVP2017), 65565, 2017.

[18] T. Yagi, K. Shinjo, S. Narita, T. Nakase and H. Shirato: Interferences of vortex sheddings in galloping instability of rectangular cylinders, *Journal of Structural Engineering*, JSCE, Vol.59A, pp.552-561, 2013.(in Japanese)

[19] Y. Nakamura and T. Mizota: Unsteady lifts and wakes of oscillating rectangular prisms, *Journal of the Engineering Mechanics Division, ASCE*, Vol.101, No.EM6, Proc. Paper 11813, pp.855-871, 1975.

[20] T. Mizota and A. Okajima: Experimental studies of flow patterns around oscillating rectangular prisms and their unsteady aerodynamic forces, *Proceedings of the Japan Society of Civil Engineers*, Vol.327, pp.49-60, 1982.(in Japanese)